Influences of Precipitation on Water Mass Transformation and Deep Convection

MICHAEL A. SPALL

ABSTRACT

The influences of precipitation on water mass transformation and the strength of the meridional overturning circulation in marginal seas are studied using theoretical and idealized numerical models. Nondimensional equations are developed for the temperature and salinity anomalies of deep convective water masses, making explicit their dependence on both geometric parameters such as basin area, sill depth, and latitude, as well as on the strength of atmospheric forcing. In addition to the properties of the convective water, the theory also predicts the magnitude of precipitation required to shut down deep convection and switch the circulation into the haline mode. High-resolution numerical model calculations compare well with the theory for the properties of the convective water mass, the strength of the meridional overturning circulation, and also the shutdown of deep convection. However, the numerical model also shows that, for precipitation levels that exceed this critical threshold, the circulation retains downwelling and northward heat transport, even in the absence of deep convection.

1. Introduction

The oceanic thermohaline circulation transports heat from low latitudes to high latitudes, transports freshwater from high latitudes to low latitudes, and plays an important role in the global heat and freshwater budgets. The ocean loses heat to the atmosphere all along its cyclonic circulation path through the subpolar North Atlantic and Nordic Seas. Heat loss can drive very deep convection in a few locations that are generally identified by weak mean circulation and a doming of isopycnals, such as the Labrador and Greenland Seas (Marshall and Schott 1999). This meridional heat transport is at least partially responsible for the warmer surface waters in the North Atlantic Ocean compared to similar latitudes in the Pacific Ocean and also leads to a relatively mild climate in Western Europe.

The possibility of fundamentally different ocean circulation patterns for an ocean driven by both heat and freshwater flux was raised by the two-box model of Stommel (1961) and again by Rooth (1982). In these simple models, there is a parameter regime for which the ocean can have more than one stable circulation state for the same atmospheric forcing. There exists a thermal mode, which is characterized by northward surface transport of warm, salty water with a cold, deep return flow (this corresponds to the present-day circulation in the North Atlantic) and a haline mode, for which the circulation transports cold freshwater equatorward near the surface. The Stommel model predicts that the thermal mode can exist for only a limited parameter space and that for sufficiently strong freshwater forcing at high latitudes the only mode that exists is the haline mode. Thus, there is concern that the present-day thermal mode might be shut down if climate change results in sufficient freshwater input in the high latitudes of the North Atlantic: for example, by increased precipitation, river runoff, or melting of the Greenland ice sheet (Broeker et al. 1985; Rahmstorf et al. 2005). Such an increase in the hydrological cycle is expected for a warming planet (Wentz et al. 2007). The existence of multiple steady states also introduces the possibility of hysteresis such that, once the system falls into the haline mode, it will remain there even subject to a reduction in the freshwater forcing below the critical level required for collapse of the thermal mode (e.g., Whitehead 1995; Marotzke 2000; Rahmstorf et al. 2005).

More complex ocean-only and coupled ocean–atmosphere general circulation models support many of the features of Stommel's original model. A sufficient increase of freshwater at the surface in the subpolar North Atlantic can lead to a shutdown of deep convection and sinking and a reduction of the oceanic meridional heat transport (Bryan 1986; Rahmstorf et al. 2005). In coupled

Corresponding author address: Michael Spall, MS#21, 360 Woods Hole Road, Woods Hole, MA 02543.
E-mail: mspall@whoi.edu

ocean–atmosphere models, this results in a cooling over the northern North Atlantic and Europe of several degrees Celsius (Manabe and Stouffer 1995; Rahmstorf 1995).

Traditional climate models are not yet able to explicitly represent mesoscale eddies or their influence on heat and freshwater transport. Mesoscale eddies are known to play a central role in closing the heat budgets in convective regions (Marshall and Schott 1999). Recent idealized modeling and theoretical studies suggest that the strength of the cyclonic boundary current systems that encircle deep convection sites are controlled by heat loss in the basin interior and the efficiency by which eddies can transport heat from the boundary current into the interior convection sites (Spall 2004, 2011). It was shown that the eddies are a central element in determining the properties of the convective water mass, the exported water mass, the meridional heat transport, and the strength of the meridional overturning circulation (MOC). These studies were limited to thermal forcing only. Straneo (2006) found that a similar model with both temperature and salinity forced by realistic atmospheric fluxes was able to reproduce much of the seasonal to interannual variability in the Labrador Sea, suggesting the relevance of the basic model dynamics.

Although the general behavior of the oceanic circulation under mixed boundary conditions has been known for a long time and is supported by a wide range of models, fundamental aspects of the dynamics remain unknown. For example, it is not well understood what determines the level of precipitation that is required to shut down deep convection. What is the influence of basin geometry (sill depth, area, and topography)? Would a warming or freshening of the ocean at low latitudes make shutdown more or less likely? Do mesoscale eddies change the basic prediction of multiple steady states and thermohaline collapse? These issues will be addressed with a combination of an analytic model (developed in section 2) and an idealized eddy-resolving general circulation model (sections 3 and 4).

2. A simple model of the marginal sea

Following Spall (2004, 2011), a simple theoretical model to determine the primary characteristics of the water mass transformation within a marginal sea is now developed. This approach builds on the results from idealized general circulation models and observations in the North Atlantic subpolar gyre and Nordic Seas. It is assumed that the heat, salt, and mass fluxes across the sill are carried by the mean flow in a cyclonic boundary current system, northward along the eastern boundary
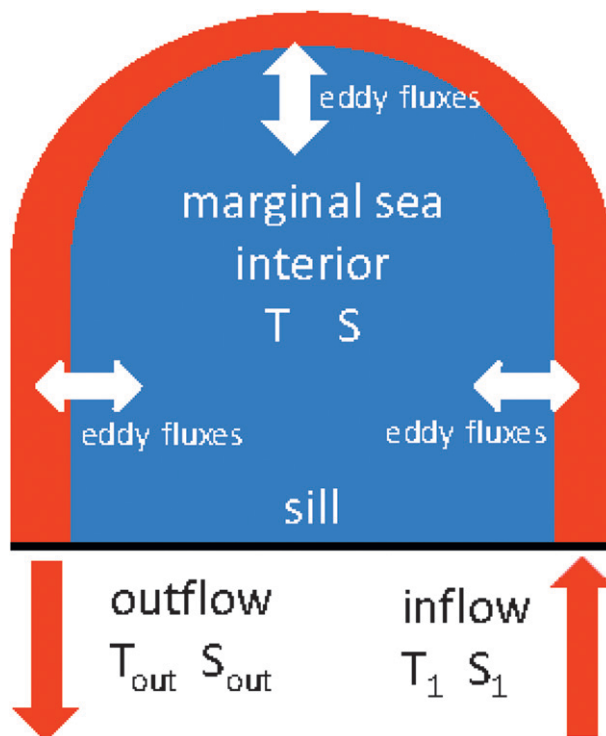

FIG. 1. Schematic of the idealized marginal sea model. The basin interior is defined by closed topographic contours while the cyclonic boundary current lies over topographic contours that connect with the open ocean. The basin interior is homogeneous with temperature T and salinity S. The inflowing water has temperature T_1 and salinity S_1, and the outflowing water has temperature T_{out} and salinity S_{out}. All exchange across the sill is carried by the mean flow, whereas all exchange between the boundary current and the basin interior is carried by eddies.

and southward along the western boundary (Fig. 1). The interior of the marginal sea, defined by a region of flat or closed topographic contours, is taken to be filled with a homogeneous water mass of temperature T and salinity S. It is assumed that the mean flow is directed along the topography and, as a result, heat and freshwater exchanges between the ocean and atmosphere in the basin interior must be balanced by lateral eddy advection from the cyclonic boundary current. Such eddy shedding is prominent in the Labrador Sea (Prater 2002; Lilly and Rhines 2002) and the Lofoten Basin of the Nordic Seas (Poulain et al. 1996). The assumption that the exchange across the sill is carried entirely by the mean flow and the exchange with the interior is carried entirely by the eddy fluxes allows for analytic progress to be made.

The properties of the convective water mass can be determined by the heat and salt balances in the basin interior. The heat flux is parameterized by a relaxation of the sea surface temperature toward an atmospheric temperature with a relaxation constant Γ (W m^{-2} C^{-1};

Haney 1971). In this way, warm water loses heat more rapidly to a cold atmosphere than does cold water. Salinity has no such strong feedback between the sea surface salinity and the freshwater flux, and so the surface condition for salinity is a specified flux E (m s^{-1}). Although Stommel (1961) used a restoring condition for salinity that was weaker than that for temperature, it is essentially this difference in boundary conditions between temperature and salinity that allows for multiple equilibria in the thermohaline circulation. The equations for the heat and salt balances in the basin interior are written as

$$PH\overline{u'T'} = \frac{A\Gamma(T - T_A)}{\rho_0 C_p} \quad \text{and} \tag{1}$$

$$PH\overline{u'S'} = -AES_0, \tag{2}$$

where T is the mean temperature in the basin interior (and S will be the mean salinity in the basin interior), the overbar denotes a time average, primes indicate perturbations from the time mean, u' is the velocity component directed into the basin interior, P is the perimeter of the interior of the marginal sea (where the topography is flat or the topographic contours are closed), A is the surface area of the interior of the marginal sea, H is the sill depth, ρ_0 is a representative ocean density, S_0 is a representative ocean salinity, E is the net evaporation minus precipitation, and C_p is the specific heat of seawater. Here, T_A is the spatial average of the atmospheric temperature over the interior of the marginal sea.

The eddy heat and salt fluxes are parameterized as being proportional to the baroclinic velocity in the inflowing boundary current V and the temperature or salinity difference between the boundary current and the basin interior (Visbeck et al. 1996; Spall 2004),

$$\overline{u'T'} = cV(T_1 - T), \quad \overline{u'S'} = cV(S_1 - S). \tag{3}$$

For simplicity, it is assumed that the temperature and salinity of the boundary current are the same as the (known) temperature and salinity of the ocean to the south of the sill along the eastern boundary, denoted as T_1 and S_1.

The coefficient c depends on the bottom slope approximately as $c = 0.025e^{2\delta}$, as derived from linear baroclinic stability theory in Spall (2004). The nondimensional parameter δ is the ratio of the bottom slope to the mean isopycnal slope in the boundary current. Isachsen (2011) tested the linear stability theory used by Spall (2004) over a wide range of bottom slopes and nonlinearity and found generally close agreement between

the theory and a nonlinear model for $-1 < \delta < 0$ (cyclonic boundary currents). For simplicity, it will be assumed that c is constant; its value is estimated empirically through comparisons with eddy-resolving numerical model results in section 3 to be $c = 0.007$. This implies $\delta = -0.64$, which is roughly consistent with the mean hydrography of the cyclonic boundary current in the model calculations and consistent with observations in the Labrador Sea (Pickart and Spall 2007).

The depth-averaged baroclinic velocity in the boundary current is assumed to be in thermal wind balance, so it depends linearly on the density difference between the boundary current and the interior,

$$V = \frac{gH}{2\rho_0 f_0 L}[\alpha_T(T_1 - T) - \alpha_S(S_1 - S)], \tag{4}$$

where g is the gravitational acceleration, α_T is the thermal expansion coefficient, and α_S is the haline expansion coefficient (a linear equation of state is used). Here, L is the width of the sloping topography over which the boundary current lies, assumed to be given by those topographic contours that connect from the open ocean into the marginal sea (Iovino et al. 2008) as $L = H/s$, where $s = 0.02$ is the average bottom slope around the perimeter of the marginal sea. It is assumed that the temperature and salinity of the boundary current are constant around the perimeter of the basin. In reality T_1, S_1, and V decrease around the perimeter of the basin as a result of exchanges with the atmosphere and basin interior. Such spatial dependence would be difficult to represent in the following analytical solution and so is neglected here.

Using these conditions, the heat and salt balances, (1) and (2), may be written as

$$\frac{gcPH^2}{2\rho_0 f_0 L}[\alpha_T(T_1 - T) - \alpha_S(S_1 - S)](T_1 - T)$$
$$= \frac{A\Gamma(T - T_A)}{\rho_0 C_p} \quad \text{and} \tag{5}$$

$$\frac{gcPH^2}{2\rho_0 f_0 L}[\alpha_T(T_1 - T) - \alpha_S(S_1 - S)](S_1 - S) = -AES_0. \tag{6}$$

It has been assumed that the density difference between the boundary current and the interior is controlled by temperature, giving rise to the thermal mode solutions. If the density difference is determined by salinity, the left-hand side of (5) and (6) change sign, resulting in the haline mode solution (discussed further below). We will solve for the nondimensional temperature

difference between the boundary current and the basin interior, $\Delta T = (T_1 - T)/T^*$, and the nondimensional salinity difference between the boundary current and the basin interior, $\Delta S = (S_1 - S)\alpha_S/\alpha_T T^*$, where salinity has been scaled by the salinity equivalent of a density anomaly of αT^*. The natural temperature scale in the problem is defined by $T^* = T_1 - T_A$, the difference between the inflowing temperature and the temperature of the atmosphere over the interior of the marginal sea.

Equations (5) and (6) may be arranged as a single equation for temperature,

$$\Delta T^2 \mp (\Delta T^2 + \gamma/\varepsilon)^{1/2}\Delta T + 4\mu/\epsilon(\Delta T - 1) = 0, \quad (7)$$

and a diagnostic equation for salinity,

$$\Delta S = \frac{1}{2}[\Delta T \pm (\Delta T^2 + \gamma/\epsilon)^{1/2}]. \quad (8)$$

Eq. (7) can also be written as a cubic, which has two positive roots and one negative root (not physically relevant here).

The nondimensional $\epsilon = cP/L$ is the ratio of the heat fluxed into the basin interior by eddies compared to that advected into the basin in the inflowing boundary current (relative to T; Spall 2004). The value of ϵ is very small for stable boundary currents and increases to 1 for boundary currents that are sufficiently unstable that they lose all their heat to the interior of the basin before it is carried all the way around the marginal sea.

The nondimensional parameter μ is defined as

$$\mu = \frac{A\Gamma f_0}{\alpha_T g C_p H^2 T^*}. \quad (9)$$

As discussed by Spall (2011), μ/ϵ is a measure of the relative influence of lateral eddy heat fluxes from the boundary current into the basin interior compared to heat loss to the atmosphere. For $\mu/\epsilon \ll 1$, lateral eddy heat flux from the boundary is very strong and leads to a relatively warm basin interior (cf. the atmospheric temperature): that is, $T \approx T_1$. For $\mu/\epsilon \gg 1$, the boundary current is relatively stable and the atmosphere is able to strongly cool the basin interior so that $T \approx T_A$.

There is now an additional nondimensional parameter γ that is proportional to the freshwater flux E,

$$\gamma = \frac{8A\rho_0 f_0 S_0 \alpha_S E}{g H^2 \alpha_T^2 T^{*2}}. \quad (10)$$

Similar to μ/ϵ, the combination γ/ϵ characterizes the relative balance between surface forcing and lateral eddy fluxes in the salinity balance. The precipitation scale defined by $\gamma/\epsilon = 1$ represents the maximum

amount of freshwater flux over the basin interior that can be balanced by lateral eddy fluxes of salt from the boundary current. For values of precipitation in excess of this amount, the maximum salt transport possible from the boundary current still cannot balance the surface forcing, and freshwater will accumulate in the basin interior. Of course, for most configurations, the system will not be able to support even this amount of an eddy salt flux. Large values of γ/ϵ indicate dominance of atmospheric forcing, and small values indicate strong lateral eddy fluxes. Note that in (7) and (8) μ and γ always appear in combination with ϵ. They are discussed as separate parameters to clarify their influences on the solutions, and they appear separately in the whole basin budgets that are required to evaluate the strength of the meridional overturning circulation below.

It can be shown that (7) and (8) are equivalent to the equations derived for a simple two-box model of the thermohaline circulation subject to a restoring condition on temperature and a flux condition on salinity (Huang et al. 1992) and are very similar in behavior to the classic two-box model of the thermohaline circulation with restoring for salinity originally developed by Stommel (1961). In this context, the boundary current plays the role of the low-latitude box and the interior of the marginal sea is analogous to the high-latitude box. The exchange between the boxes in the previous box models was assumed to be due to mean advection down the pressure gradient. This causes some conceptual difficulty if one thinks the large-scale mean flow is in geostrophic balance (flow along constant pressure). However, here the heat and salt transports are driven by eddy fluxes, which one would expect to be in the direction of the pressure gradient if they are a result of baroclinic instability [e.g., (3) and (4)]. The mean transport down the pressure gradient in the previous box models was interpreted as the strength of the overturning circulation. However, in the present model, this is really the diapycnal mass flux carried by mesoscale eddies. As will be shown below, this is very different from the overturning mass flux.

This model is similar to the two-box model in the appendix of Marotzke (2000), although his model predicted only the salinity. His equation (5) is equivalent to (8) but, because temperature is fixed in his model, there is no equivalent to (7). The present model also has similarities with the two-box models of Welander (1982), Rahmstorf (2001), and Kuhlbrodt et al. (2001), in which convection is represented by a seasonal mixed layer and a deep convective water mass. The deep-ocean properties are fixed in the model of Welander, and exchange between the deep ocean and the surrounding water masses is parameterized by a restoring to a specified temperature and salinity by Rahmstorf (2001) and Kuhlbrodt et al. (2001).

This restoring represents exchange between the convection region and the surrounding ocean, analogous to the eddy flux exchange represented by (3). A key difference is that the exchange coefficient in the present model is not a constant; it depends on the density difference between the boxes and also on the geometry and topography of the basin. Stigebrandt (1985) also introduced a simple model of a heat and freshwater forced marginal sea with a sill that consisted of a geostrophically balanced cyclonic boundary current and a homogeneous basin interior. The configuration was very similar to the present one, but the explicit exchange between the boundary current and the basin interior due to eddies and the dependence of heat flux on ocean temperature were not considered; thus, the system was underdetermined.

The present system of equations supports two solutions (the thermal modes) reflected by the $\pm$ in (8). The positive root in (8) [which corresponds to the negative root in (7)] results in steady solutions for which $\Delta S > 0.5\Delta T$, although it can be shown that most of these solutions are unstable to small perturbations and are thus inaccessible in time-dependent configurations. The other root produces steady, stable solutions in which the density contrast is dominated by the temperature difference. These are the stable and unstable thermal modes discussed by Stommel (1961) and others.

The haline mode results if the salinity contribution is larger than the density contribution, $\Delta S/\Delta T > 1$, in which case the water in the interior of the marginal sea is less dense than that in the boundary current. The sense of the boundary current circulation is reversed, resulting in a change of sign for the terms with μ/ϵ and γ/ϵ. The resulting equations for the haline mode are

$$\Delta T^2 - (\Delta T^2 - \gamma/\epsilon)^{1/2}\Delta T - 4\mu/\epsilon(\Delta T - 1) = 0 \quad \text{and} \quad (11)$$

$$\Delta S = \frac{1}{2}[\Delta T + (\Delta T^2 - \gamma/\epsilon)^{1/2}]. \quad (12)$$

There is only one root that gives a physically consistent solution with $0 < T < 1$. It has been surmised that the present thermal mode of circulation in the North Atlantic Ocean might flip into the haline mode of circulation if sufficient freshwater is introduced at high latitudes, the so-called thermohaline catastrophe (Broeker et al. 1985). This will be discussed further below; for the remainder of this section, we will concentrate on the stable thermal mode solution.

a. Temperature and salinity of the convective water mass

The coupled set of equations (7) and (8) can be solved numerically for the stable thermal mode given specified values of the forcing parameters μ/ϵ and γ/ϵ. The nondimensional temperature difference between the inflowing water and the convective water mass in the interior of the marginal sea is shown in Fig. 2a over a wide range of forcing parameters. For weak thermal forcing, $\mu/\epsilon \ll 1$, $\Delta T \ll 1$, meaning that the temperature in the interior of the basin is close to the temperature of the inflowing water along the eastern boundary. The eddies are able to flux a lot of heat into the basin interior before the atmosphere can cool the ocean. The temperature in the basin interior decreases with increasing μ/ϵ, with ΔT approaching 1 for $\mu/\epsilon \gg 1$. The temperature of the convective water mass is only weakly dependent on the strength of freshwater forcing γ/ϵ, becoming slightly cooler as precipitation is increased.

For sufficiently strong precipitation such that $\gamma/\epsilon < -\Delta T^2$, the discriminant in (7) and (8) will become negative. This gives rise to imaginary roots for ΔT and ΔS. It has been assumed in the derivation of the heat and salt budgets that the interior consists of a homogeneous water mass that exchanges heat and fresh with the atmosphere, which is balanced by lateral eddy fluxes from the boundary current. The salinity acts to reduce the density difference between the boundary current and the basin interior, thus reducing the strength of the eddy fluxes originating from the boundary current [see (3) and (4)]. If the temperature contrast is too small, the eddy fluxes are unable to balance the precipitation in the basin interior and steady, convective solutions are not possible. This nonconvective regime is indicated by the white region in Fig. 2. Increasingly large values of precipitation are required to shut down convection as the thermal forcing gets stronger (or the eddy fluxes get weaker, large μ/ϵ). The definitions of μ, γ, and ϵ explicitly demonstrate the dependence of convective shutdown on all model parameters, including basin geometry (sill depth, area, and topographic slope), the relative difference between the ocean and atmospheric temperature, the strength of thermal relaxation, and the Coriolis parameter. Note that, because of the linear equation of state and the constant reference salinity in (2), the salinity of the inflowing water does not influence the equilibrium state of the system.

For the traditional two-box model of Stommel (1961), precipitation exceeding this critical value results in a switch from the thermal mode to the haline mode. The nature of the solutions in this limit will be explored using a numerical model in section 4. The main point here is that a finite regime defined by the values of γ/ε and μ/ϵ exists for which the system can support deep convection in the basin interior.

The salinity difference between the boundary current and the basin interior is shown in Fig. 2b. The interior becomes fresher as γ/ε becomes increasingly negative, as expected. Salinity is a weak function of thermal forcing
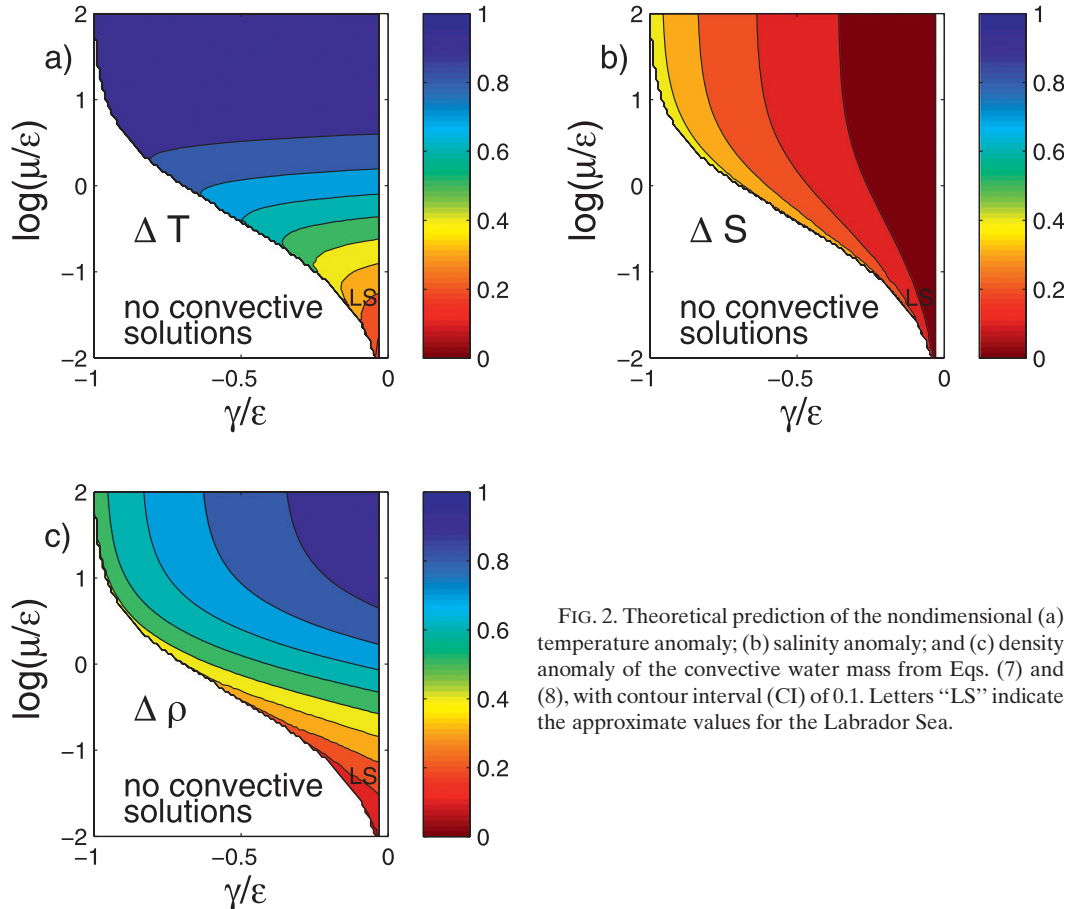
FIG. 2. Theoretical prediction of the nondimensional (a) temperature anomaly; (b) salinity anomaly; and (c) density anomaly of the convective water mass from Eqs. (7) and (8), with contour interval (CI) of 0.1. Letters "LS" indicate the approximate values for the Labrador Sea.

away from the limit of deep convection but becomes a stronger function of μ/ϵ as this limit is approached. At the limit of deep convection, $\Delta S = \Delta T/2$. The contribution of salinity to the density difference between the boundary current and the basin interior cannot exceed half that of the temperature difference. The relative proximity of any convective basin to haline catastrophe can be estimated from hydrography by $\Delta S/\Delta T$.

The density difference between the boundary current and the basin interior is $\Delta T - \Delta S$, as shown in Fig. 2c. The density anomaly of the convective water mass is only a weak function of γ/ϵ for $\mu/\epsilon \ll 1$ but depends only on γ/ϵ for $\mu/\epsilon \gg 1$.

Values of μ/ϵ and γ/ϵ can be estimated for the Labrador Sea. Although the uncertainties are large, it is nonetheless useful to give an idea of where this region of deep convection lies in nondimensional forcing space and to assess the predictions from the theory. The area of the interior of the Labrador Sea is approximately 5×10^{11} m^2 and the Coriolis parameter $f_0 = 1.2 \times 10^{-4}$ s^{-1}. The restoring constant Γ is set to 10 W m^{-2} C^{-1} (Seager et al. 1995). The annual-mean atmospheric temperature is approximately $T_A = 0°$C [calculated from the European

Centre for Medium-Range Weather Forecasts (ECMWF) Interim Reanalysis (ERA-Interim) data of Dee et al. 2011], whereas the inflowing water temperature is approximately 4.5°C (Pickart and Spall 2007), giving $T^* = 4.5°$C. The vertical-scale height $H = 1500$ m is taken to be the approximate depth of the Nordic Seas overflow water in the Labrador Sea. This is of course not the same as the sill depth assumed in the theory and could be a different depth for different parameter regimes, so it must be viewed as an empirical factor for this parameter estimate. The thermal expansion coefficient $\alpha_T = 0.15$ kg m^{-3} C^{-1}. The net evaporation minus precipitation rate for the Labrador Sea is approximately 1.5×10^{-8} m s^{-1} (Schanze et al. 2010). The eddy flux parameter ε was estimated to be 0.2 by Pickart and Spall (2007). The resulting values are $\mu/\epsilon = 0.05$ and $\gamma/\epsilon = 0.1$, which lies in the lower-right region of parameter space, as indicated by the letters in Fig. 2. The predicted properties for the convective water mass in the Labrador Sea are $T_1 - T = 1.5°$C and $S_1 - S = 0.11$. Although inputs to these estimates are not well constrained, the main point is that the theory gives predictions that are in reasonable agreement with observations (e.g., in the

averaged hydrographic data in Pickart and Spall 2007) and that most oceanographically relevant regions will have $\mu/\epsilon \lesssim O(1)$. The ratio $\Delta S/\Delta T = 0.4$ is reasonably close to the critical value of 0.5, suggesting that the Labrador Sea might be vulnerable to a shutdown of deep convection. Kuhlbrodt et al. (2001) also concluded that the Labrador Sea is close to a state that cannot support deep convection.

b. Overturning in the marginal sea

The amount of sinking driven by buoyancy forcing in the marginal sea is a fundamental quantity that characterizes the general circulation and water mass transformation. These dense waters also form the overflow waters that would pass over the sill and entrain significant ambient water as they flow downslope to the south. Understanding what determines the amount of sinking within the marginal sea is important if we are to understand and predict the ocean response to changes in atmospheric forcing at high latitudes or changes in the properties of waters flowing into the marginal sea.

The net sinking in the marginal sea can now be calculated by applying heat and salt budgets over the entire marginal sea. Following Spall (2011), it is assumed that the mass and heat exchange between the marginal sea and the open ocean are carried by the mean, geostrophically balanced flow in the eastern and western boundary currents and that the inflowing mass transport is balanced by the outflowing mass transport. The outflowing water must be denser than the inflowing water in order to balance the buoyancy loss to the atmosphere. Thermal wind balance then requires that the vertical shear in the outflowing boundary current is less than the vertical shear in the inflowing boundary current. This in turn requires that mass downwell somewhere within the marginal sea in order to maintain geostrophic balance. Detailed studies of the dynamics of these downwelling regions indicate that they are concentrated near the boundaries where the boundary current loses heat either directly to the atmosphere or laterally via eddy fluxes (Spall 2010; Cenedese 2012).

For the present analysis, we seek only to understand what controls the net downwelling within the marginal sea. Thermal wind balance indicates that the change in the vertical shear between the inflowing and outflowing boundary currents is proportional to the density difference between the eastern and western boundaries. The net downwelling within the basin is given by the change in geostrophic transport required to balance this density change over one-half the sill depth. The one-half enters because the transport loss in the upper half of the water column is gained in the lower half of the water column,

thus reducing the vertical shear in the boundary current. The magnitude of the downwelling required is

$$W^* = 0.5(V - V_{out})HL = \frac{gH^2(\rho_1 - \rho_{out})}{4\rho_0 f_0}, \quad (13)$$

where the subscript "out" refers to the property of the outflowing boundary current.

Heat and salt balances for the entire marginal sea may be written as

$$(T_1 - T_{out})VHL = \frac{A\Gamma}{\rho_0 C_p}[T - T_A + PL/A(T_1 - T_A)]$$

and

$$(14)$$

$$(S_1 - S_{out})VHL = -EAS_0. \quad (15)$$

For simplicity, it has been assumed in (15) that the area over the boundary current is negligible compared to the area of the interior of the marginal sea. Equations (14) and (15) may be combined with (4), (7), (8), and (13) to obtain the nondimensional downwelling within the basin,

$$W = W^*/\Psi = \frac{1}{2\Delta\rho}(2\mu(1 - \Delta T + PL/A) + \gamma/4). \quad (16)$$

The downwelling has been nondimensionalized by the maximum baroclinic transport that the circulation can support, $\Psi = gH^2\alpha_T T^*/2\rho_0 f_0$. The term $1 - \Delta T$ results from heat loss in the basin interior and the term PL/A accounts for heat loss directly from the boundary current to the atmosphere. The latter term is generally small but can become important for $\mu/\epsilon \gg 1$, where $\Delta T \to 1$. Neglecting this term, the downwelling may be written as

$$W = 0.5\epsilon(\Delta T - \Delta S). \quad (17)$$

This surprisingly simple expression shows that the net downwelling within the marginal sea depends explicitly on the parameter ϵ, which is a measure of how much heat and salt are lost from the boundary current into the basin interior because of lateral eddy fluxes. The other component is the density anomaly of the convective water mass ($\Delta\rho = \Delta T - \Delta S$), which determines the horizontal transport in the boundary current through the thermal wind relation. The influence of atmospheric forcing on the downwelling within the marginal sea is then indicated by $\Delta\rho$, which is shown in Fig. 2c. For weak thermal restoring (small μ/ϵ), the meridional overturning circulation in the marginal sea is only weakly dependent on precipitation, but it is strongly dependent on changes in thermal forcing. In the less realistic limit of large μ/ϵ, the

net sinking is entirely controlled by precipitation because the temperature of the convective water is essentially constant at the atmospheric temperature. Precipitation also becomes more important as the limit of convective solutions is approached. The expression for downwelling within the basin derived by Spall (2011) is consistent with this result for $\Delta S = 0$, although it is not easily inferred from the expression given in that paper.

3. Comparisons with an eddy-resolving numerical model

The theory derived above for the properties of water mass transformation in a marginal sea made use of simple dynamic and thermodynamic assumptions. However, it is possible that one or more of those assumptions are not well satisfied in a more realistic model that includes non-linearities, time dependence, and explicitly resolved mesoscale eddies. In this section, an eddy-resolving ocean circulation model is configured in an idealized basin and subject to wind stress and heat and freshwater flux forcing. The advantage of the idealized configuration is that the nondimensional numbers μ and γ can be readily calculated and systematically varied in order to test the basic parameter dependencies predicted by the theory. If good agreement is found, the physical understanding that derives from the analytic solutions can be directly applied to the more complete general circulation represented by the numerical model.

The numerical model is the Massachusetts Institute of Technology General Circulation Model (MITgcm; Marshall et al. 1997), details of the model domain and forcing are given in the appendix and Fig. 3. The configuration is the same as in Spall (2011) except that in addition to a surface heat flux represented by a restoring of sea surface temperature to an atmospheric temperature, a virtual salt flux is prescribed in the marginal sea, north of 1200-km latitude.

The model is started at a state of rest with an initial stratification of $N^2 = 2 \times 10^{-6}$ s^{-2} and upper-level temperature of 10°C. For this calculation, the sill depth is 1000 m, the atmospheric restoring strength is 10 W m^{-2} C^{-1}, and precipitation $E = -2 \times 10^{-8}$ m s^{-1} north of 1200-km latitude. The model is run for a period of 30 yr for most of the calculations described below, which is sufficient to achieve a statistical steady state (as indicated by basin-integrated available potential energy or kinetic energy and also the quantities diagnosed below). This rapid spinup time results from a full depth restoring near the southern boundary that is intended to represent warming and upwelling in the rest of the World Ocean, as discussed by Spall (2011). Note that this neglects any feedback between water mass transformation
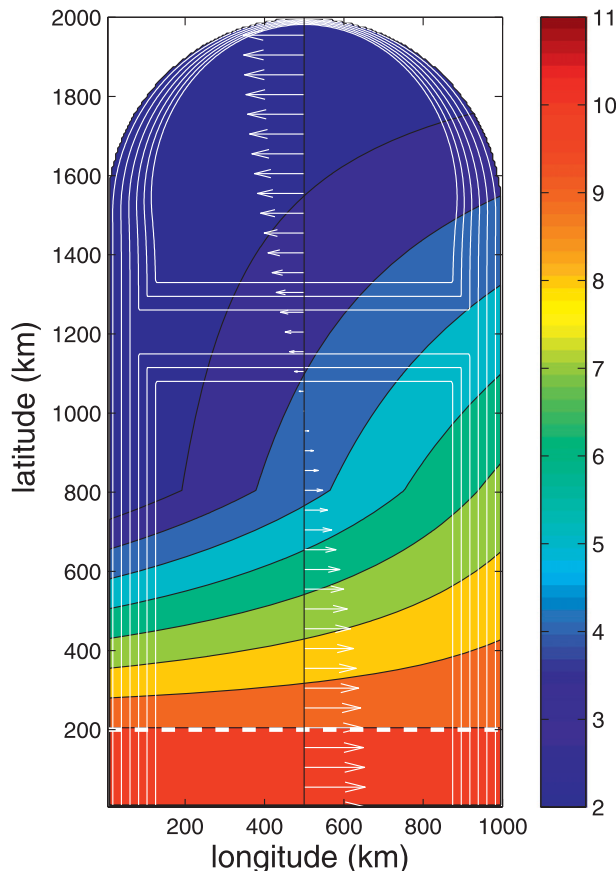

FIG. 3. Model domain, bottom topography (white contours; CI = 300 m), wind stress (vectors), and atmospheric temperature toward which the model sea surface temperature is restored (colors). Temperature is restored toward a uniform stratification, and salinity is restored toward 35, in the region south of the bold dashed white line at 200 km. Precipitation is nonzero over the entire region north of the sill at 1200-km latitude.

at high latitudes and the stratification at low latitudes. Specifically, solutions for which low-latitude diapycnal mixing and the upwelling branch of the MOC decrease with increasing stratification (Nilsson and Walin 2001) are not considered. This low-latitude restoring toward a uniform stratification may also inhibit the development of the haline mode, in which the sense of the over-turning circulation is sinking in the south and upwelling in the north.

Although clearly very idealized compared to the real ocean, the model represents several key aspects of the observed circulation in the northern North Atlantic Ocean and Nordic Seas. The mean basin-scale circulation is cyclonic in both the central and northern basins (Fig. 4). Warm, salty water is advected northward along the western boundary at low latitudes, crosses the basin in the middle of the southern basin, and continues northward along the eastern boundary. Upon reaching
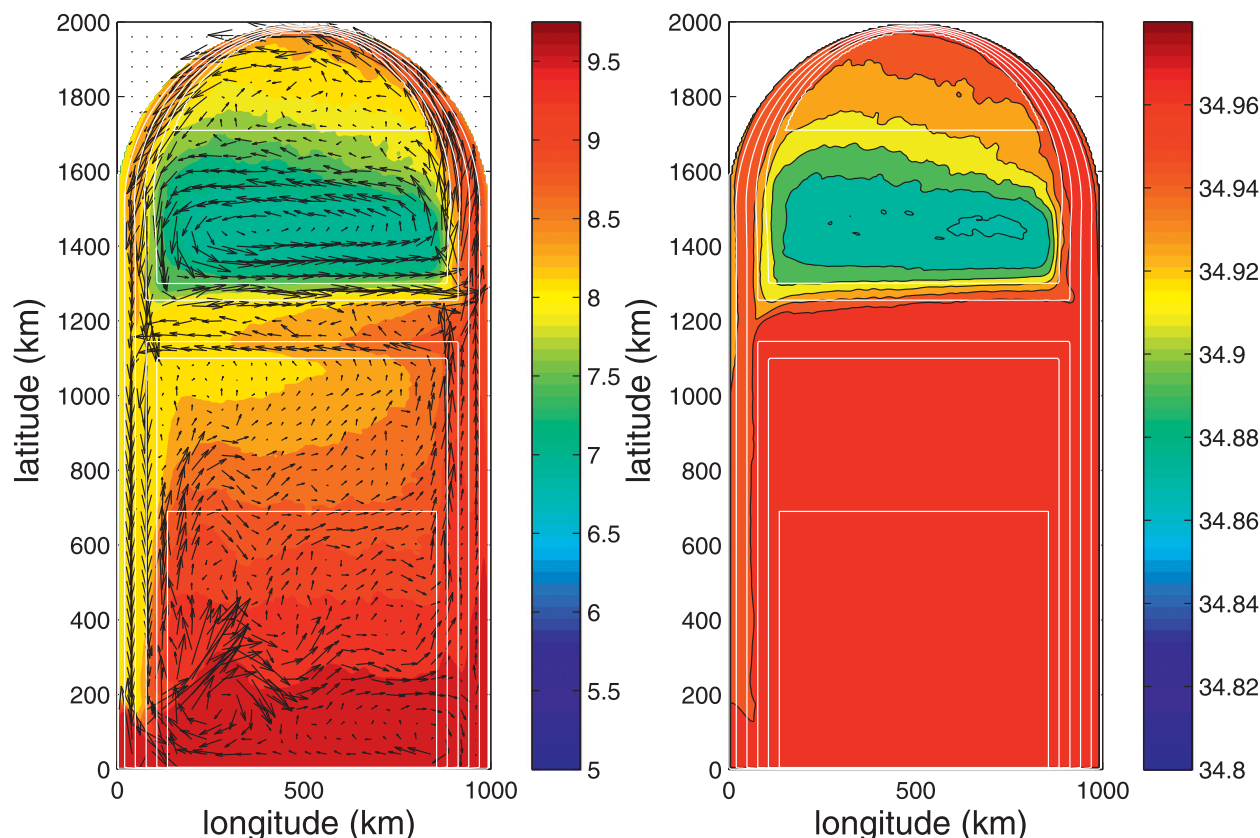
FIG. 4. (left) Mean sea surface temperature and horizontal velocity (every eighth grid point). (right) Mean sea surface salinity. White contours are the bottom topography, with a CI of 400 m.

the sill at 1200-km latitude, the warm current splits into two branches, with one flowing to the west along the southern flank of the sill and the other continuing toward the north into the marginal sea. A similar branching south of the sill is seen in observations (Orvik and Niiler 2002). The temperature decreases monotonically along both pathways as a result of heat loss to the atmosphere and lateral eddy fluxes into the basin interior. The salinity also decreases cyclonically around the marginal sea because of precipitation. The coldest and freshest waters in the model are found in the center of the marginal sea. The water flowing southward along the western boundary of the marginal sea is colder and fresher than the northward-flowing water along the eastern boundary but is not as cold and fresh as the convective waters in the interior of the marginal sea.

a. Water mass properties

The predictions for the properties of the convective water mass from the theory in section 2 are now compared to properties diagnosed from a series of numerical model calculations, as summarized in Table 1. The basic circulation pattern in Fig. 4 is found for a wide range of thermal

and freshwater forcing strengths. For this model forcing (run 2), $\mu/\epsilon = 0.057$. The magnitude of γ/ϵ is varied by increasing the precipitation over the marginal sea, giving a range of $\gamma/\epsilon = 0, -0.08, -0.12, -0.14, -0.16$, and -0.20 (Table 1). The nondimensional temperature and salinity anomalies of the interior convective water mass are calculated as $\Delta T = (T_1 - T)/T^*$ and $\Delta S = (S_1 - S)\alpha_S/\alpha_T T^*$, where the subscript 1 indicates the transport weighted inflowing temperature and salinity along the eastern boundary and T and S indicate the average sea surface temperature and salinity over the final 5 yr of model integration in a circular region of 200-km diameter centered at 500-km longitude and 1550-km latitude. The solid line in Fig. 5 indicates the theoretical temperature and the dashed line is the theoretical salinity from (7) and (8). The thick line indicates the stable thermal mode solutions while the thin lines are the unstable thermal mode. The dotted and dashed–dotted lines indicate the salinity and temperature for the haline mode. It is evident that the unstable thermal mode has a much smaller density difference between the boundary current and the interior, which implies a weaker geostrophic flow in the boundary current and eddy flux into the interior. The asterisks mark

TABLE 1. Summary of model runs with key parameters: sill depth H (m); relaxation constant Γ (W m^{-2} C^{-1}); temperature anomaly of inflowing water T^*; thermal forcing μ/ϵ; precipitation E (10^{-8} m s^{-1}); and freshwater forcing parameter γ/ϵ. The model-diagnosed quantities are temperature anomaly of the convective water mass ($T_1 - T$; °C); salinity anomaly of the convective water mass ($S_1 - S$); and the maximum meridional overturning strength at the sill W (10^6 m^3 s^{-1}). Those calculations with no value for the temperature and salinity anomalies do not maintain deep convection in the basin interior.

RUN	H	Γ	T^*	μ/ϵ	E	γ/ϵ	$T_1 - T$	$S_1 - S$	W
1	1000	10	6.5	0.057	0.0	0.0	1.70	0.0	3.5
2	1000	10	6.5	0.057	−2.0	−0.08	1.91	0.10	3.5
3	1000	10	6.5	0.057	−3.0	−0.12	2.15	0.17	3.3
4	1000	10	6.5	0.057	−3.5	−0.14	2.26	0.22	3.2
5	1000	10	6.5	0.057	−4.0	−0.16	2.47	0.29	3.0
6	1000	10	6.5	0.057	−5.0	−0.20			2.5
7	1000	10	6.5	0.057	−10.0	−0.41			2.0
8	600	40	6.0	0.44	0.0	0.0	3.45	0.0	8.9
9	600	40	6.0	0.44	−2.5	−0.21	3.78	0.045	8.3
10	600	40	6.0	0.44	−4.0	−0.34	3.93	0.088	8.1
11	600	40	6.0	0.44	−5.0	−0.43	4.16	0.12	8.0
12	600	40	6.0	0.44	−6.0	−0.51			4.9
13	600	40	6.0	0.44	−10.0	−0.86			3.6
14	600	40	6.0	0.44	−12.0	−1.02			3.9
15	1000	4	6.8	0.022	0.0	0.0	1.45	0.0	1.4
16	1000	4	6.8	0.022	−1.0	−0.04	1.61	0.033	1.3
17	1000	4	6.8	0.022	−2.0	−0.07	1.84	0.073	1.2
18	1000	4	6.8	0.022	−3.0	−0.11			1.2
19	1000	4	6.8	0.022	−5.0	−0.19			1.1

the temperature, and the squares mark the salinity, diagnosed from the series of model runs as a function of γ/ϵ. There is generally good agreement between the model and the theory. As precipitation increases, the salinity of the convective water decreases (the anomaly increases), as expected. The temperature of the convective water also decreases with increasing precipitation but not by as much (in density units) as does salinity, so the density anomaly of the convective water decreases. For no precipitation, the temperature anomaly of the convective water is 1.7°C while, for precipitation of $E = -4 \times 10^{-8}$ m s^{-1}, the temperature anomaly increases to 2.47°C and the salinity anomaly is 0.29. This gives a ratio $\Delta S/\Delta T = 0.47$, close to the theoretical limit of 0.5.

The response to increasing precipitation for stronger thermal restoring is shown in Fig. 5b for $\mu/\epsilon = 0.44$ (sill depth of 600 m; restoring strength $\Gamma = 40$ W m^{-2} C^{-1}; runs 8–11). Once again there is reasonable agreement between the model and the theory. Deep convection is supported for larger values of γ/ϵ, as predicted by the theory. The interior is colder than for the weaker thermal forcing in Fig. 5a for all values of precipitation.

For weaker thermal restoring (sill depth of 1000 m; $\Gamma = 4$ W m^{-2} C^{-1}; $\mu/\epsilon = 0.022$; runs 15–17), the theory and model also compare closely. The temperature anomaly of the interior water mass is reduced to only

about 20% of T^* (Fig. 5c), compared to about 60% T^* for the calculation with $\Gamma = 40$ W m^{-2} C^{-1}. For this weaker restoring, the magnitude of precipitation that shuts down convection is also reduced to only about -2×10^{-8} m s^{-1}, close to that in the Labrador Sea.

b. Meridional overturning strength

Comparisons are now made between the theory and model calculations for the density anomaly of the convective water mass and the strength of the meridional overturning circulation. The density anomaly of the convective water mass (nondimensionalized by $\alpha_T T^*$) is shown in Fig. 6a for the numerical model (asterisks) and the theory (stars). There are three sets of symbols, one for each value of μ/ϵ. The agreement between model and theory is generally close. The density anomaly of the convective water increases with increasing μ/ϵ, as expected from the theory. The density anomaly decreases with increasing precipitation (γ/ϵ), only slightly for large μ/ϵ but more so for very weak thermal forcing.

The maximum meridional overturning transport at the sill latitude is indicated in Fig. 6b, nondimensionalized by the reference transport $gH^2\alpha_T T^*/2\rho_0 f_0$. This is the transport that a current would have for a lateral density change of $\alpha_T T^*$ over a depth H, the largest baroclinic transport that could be supported to flow over the sill. The model downwelling was calculated from the average of the maximum meridional overturning streamfunction at the sill latitude over the final 5 yr of model integration. Again there is close agreement between the model and theory. The meridional overturning strength is only weakly dependent on precipitation, especially so for the larger values of μ/ϵ. This result also shows that the magnitude of the downwelling is relatively small compared to the potential horizontal transport implied by the depth of the sill and the temperature of the atmosphere relative to the ocean.

4. Shutdown of deep convection

One of the basic predictions of the theory is the magnitude of precipitation that is required to shift from a regime with persistent deep convection to a regime where a freshwater cap develops in the basin interior. The state found in the model for each of the above calculations is indicated in Fig. 7 as a function of μ/ϵ and γ/ϵ. According to the theory, parameter values to the right of the curve support statistically steady solutions with deep convection in the basin interior. Such solutions are not possible to the left of the curve. The asterisks mark the location for each model calculation in which deep convection is consistently found. The circles mark the model runs for which a freshwater cap forms in
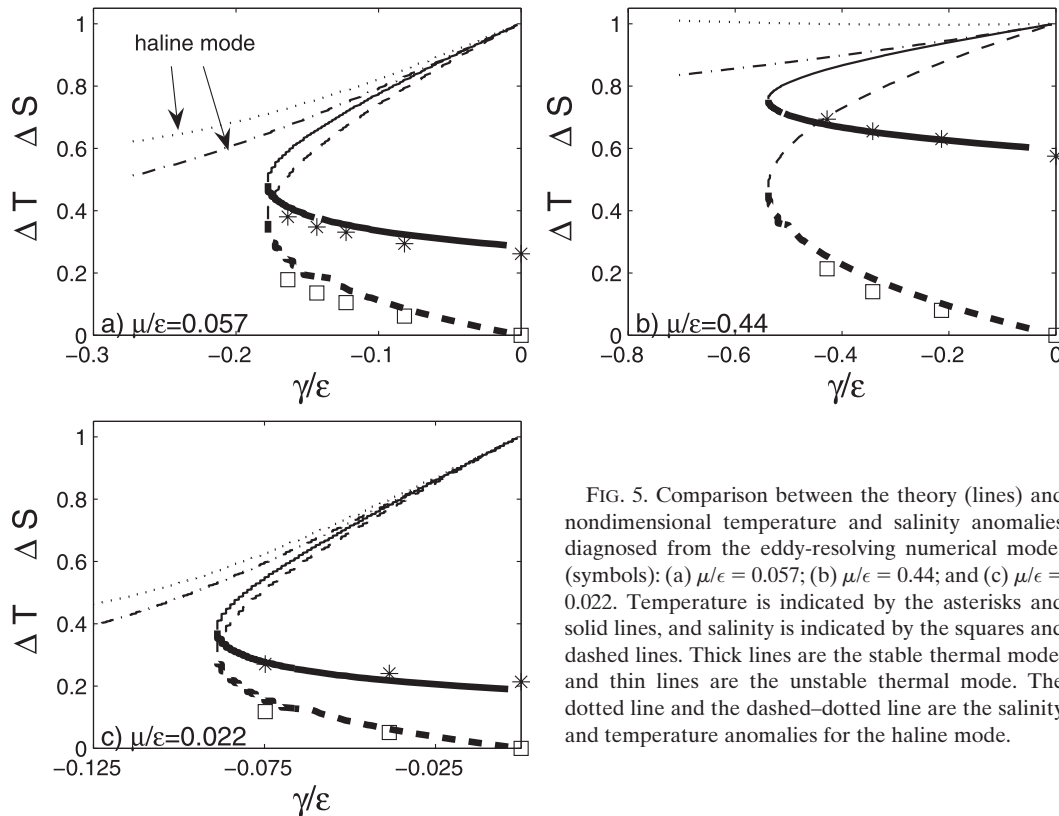
FIG. 5. Comparison between the theory (lines) and nondimensional temperature and salinity anomalies diagnosed from the eddy-resolving numerical model (symbols): (a) $\mu/\epsilon = 0.057$; (b) $\mu/\epsilon = 0.44$; and (c) $\mu/\epsilon = 0.022$. Temperature is indicated by the asterisks and solid lines, and salinity is indicated by the squares and dashed lines. Thick lines are the stable thermal mode, and thin lines are the unstable thermal mode. The dotted line and the dashed–dotted line are the salinity and temperature anomalies for the haline mode.

the interior. The transition is predicted quite well by the theory, in particular its dependence on μ/ϵ. For $\mu/\epsilon \ll 1$ (weak thermal restoring or strong eddy fluxes from the boundary), relatively weak precipitation can shut down convection, whereas convection persists for stronger values of precipitation when thermal restoring is strong.

Note that to the left of the curve the basic stratification in the marginal sea is fundamentally different than it is to the right of the curve. To the right of the curve, the marginal sea consists of a weakly stratified, cold, and fresh interior surrounded by a stratified, warm, and salty cyclonic boundary current. To the left of the curve, the interior has a cold and fresh thin cap overlying a weakly stratified interior. There still exists the warm and salty cyclonic boundary current. The deep interior is cold and fresh, although not as cold or fresh as the surface layer. This is at least partly due to the spinup process in the model, during which time the initially warm interior cools before the freshwater cap can develop. The haline mode solutions from the theory would have a homogeneous cold and fresh interior that is lighter than the surrounding boundary current, resulting in an anticyclonic direction of flow around the marginal sea. Numerous attempts were made to obtain this sense of circulation and hydrography in the model, but the solution always went to the cyclonic flow with a shallow freshwater cap in the

interior. This should not be interpreted as evidence that the haline mode cannot be supported in the numerical model, only that time stepping the model from (a relatively small number of) initial conditions, with a restoring of temperature and salinity near the southern boundary, has not produced a haline mode.

The critical value of precipitation that is required to shut down deep convection depends on several parameters of the system. For example, both μ and γ depend on the relative temperature difference between the ocean to the south of the sill and the atmosphere over the marginal sea. A freshwater cap in the marginal sea can develop if the value of T^* sufficiently decreases. It is somewhat counterintuitive that colder inflowing water would inhibit deep convection, although it is consistent with the notion that a warmer atmosphere, which also leads to smaller T^*, can lead to a shutdown of convection. Two additional calculations have been carried out with parameters identical to run 2 in Table 1, except that the temperature profile to which the model is restored in the southern 200 km of the domain was decreased by 3° and 4°C. The temperature of the inflowing water was thus decreased, resulting in values of $T_1 = 6.9°$ and 6.2°C ($T^* = 4.1°$ and 3.4°C). This increased μ/ϵ and, even more so, γ/ϵ [see (9) and (10)]. The final state of the model integration (convection or no convection) is indicated in
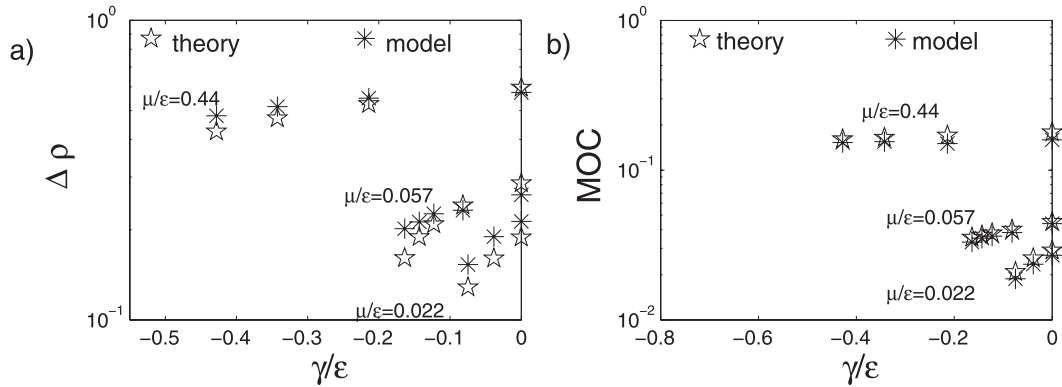
FIG. 6. (a) Density anomaly of the convective water mass. (b) Maximum strength of the MOC at the sill latitude for the three sets of model calculations with different μ/ϵ. Asterisks are diagnosed from the numerical model, and stars are predicted by the theory.

Fig. 8 by the symbols along the solid line. The star at $\mu/\epsilon = 0.057$ and $\gamma/\epsilon = 0.08$ is the standard model run 2. The state moves toward shutdown for $T^* = 4.1°C$ and crosses the critical value of γ/ϵ for $T^* = 3.4°C$. The model does not support deep convection in this case, consistent with the theory, even though precipitation has not changed and the inflowing water is more dense. This is because the density change between the boundary current and the interior is reduced (Fig. 2c), which also reduces the eddy fluxes from the boundary current into the interior. Eddy fluxes are required to maintain deep convection because this is the only way to get the high-salinity water into the interior to balance the precipitation in the basin interior.

The influence of sill depth on the loss of deep convection is demonstrated by two additional calculations with sill depths of 450 and 200 m and other parameters identical to run 2 (dashed–dotted line in Fig. 8). A reduction in sill depth decreases the strength of the inflowing boundary current via thermal wind [Eq. (4)] so that the eddy flux of salt into the basin interior is also decreased. This makes the basin more vulnerable to a shutdown of deep convection because the supply of salty water required to balance precipitation is reduced. For a sill depth of 200 m, the critical value is crossed and deep convection ceases.

A final sensitivity is examined in which the restoring strength to atmospheric temperature is decreased to 4.8 and 3 W m^{-2} C^{-1} (dashed line). In this case, γ/ϵ remains nearly constant but μ/ϵ decreases. For such weak restoring, the interior of the basin remains relatively warm and the density contrast between the boundary current and the interior relatively small. As a result, the lateral eddy fluxes from the boundary current into the interior are weak and, at the weakest restoring strength, there is insufficient flux of high-salinity water to balance

the precipitation. The model does not support deep convection in this case.

Values of precipitation that slightly exceed the critical threshold can result in a shutdown of deep convection with occasional episodes of overturning. The standard model configuration with the 600-m sill depth and $\Gamma = 40$ W m^{-2} C^{-1} was run for 200 yr with $E = -6 \times 10^{-8}$ m s^{-1} (run 12: the circle in Fig. 7 for $\mu/\epsilon = 0.44$, $\gamma/\epsilon = 0.51$). This is close to the theoretical prediction of the magnitude of precipitation that will cause the system to switch to the thermal mode. A time–depth plot of the temperature and salinity in the basin interior is shown in Fig. 9. Indeed, it is found that deep convection is not maintained in the basin interior. A freshwater cap with $S \approx 33$ develops early in the integration. The surface
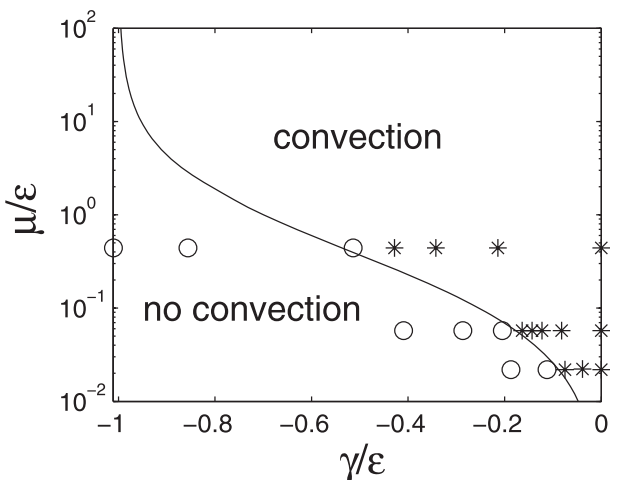

FIG. 7. The transition between the convective regime and the nonconvective regime predicted by the theory (solid line). Parameter values to the left of the line cannot support deep convection. Symbols indicate the final state of the numerical model, asterisks indicate convection, and circles indicate a freshwater cap.
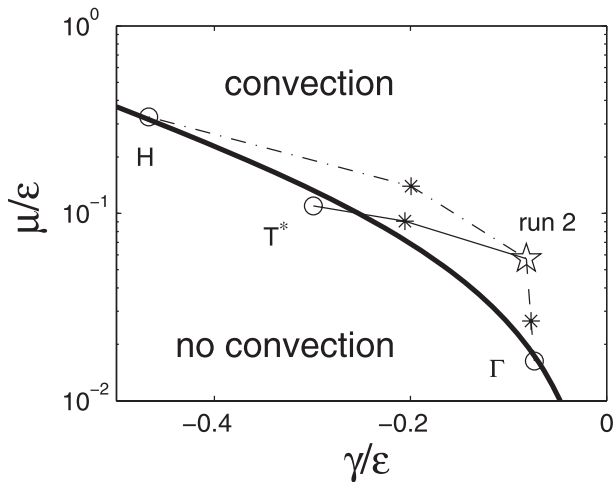
FIG. 8. The transition between the convective regime and the nonconvective regime predicted by the theory (bold solid line) and for several model calculations. The star is run 2 in Table 1; asterisks indicate convection, and circles indicate a freshwater cap. Solid line indicates $T^* = 6.9°$ and $6.2°C$; dashed–dotted line indicates $H = 450$ and 200 m; and dashed line indicates $\Gamma = 4.8$ and 3 W m^{-2} C^{-1}. All other parameters are as for run 2.

temperature becomes very cold (essentially T^*), but the middepth warms steadily. However, even in the absence of deep convection, the model maintains the same sense of circulation, with warm, salty water being carried northward into the marginal sea in an eastern boundary current. This warm boundary current loses heat directly to the atmosphere, resulting in dense water formation and downwelling. It is this boundary current that also supplies heat to the basin interior. Because the freshwater is confined to the near surface, the bulk of the basin interior remains colder and more dense than the inflowing water in the boundary current. As a result, the boundary

current remains baroclinically unstable and continues to shed eddies into the basin interior (Fig. 10). Because the freshwater cap has shut down deep convection, the heat remains isolated from the atmosphere. Figure 9 bears some resemblance to the evolution of temperature and salinity in the interior of the Labrador Sea during the years of the Great Salinity Anomaly when deep convection was shut down (Straneo 2006). In the model, the continued eddy fluxes from the boundary eventually warm the basin interior sufficiently that the deep water becomes lighter than the fresh (and cold) surface layer and the interior overturns, restarting deep convection. However, the freshwater starts to accumulate at the surface once again and the cycle restarts. Several of these capping–flushing cycles occur over the 200-yr simulation (around years 80, 120, and 170).

A time series of the meridional overturning strength, the meridional heat transport at the sill latitude, and the area of deep mixed layers (defined as exceeding 1000 m) north of the sill are shown in Fig. 11. The flushing events indicated in Fig. 9 are evident by periods of deep mixed layers. The meridional overturning maintains its positive sense throughout the 200-yr integration, with enhanced strength during the time periods of deep convection. However, even during the decades when there is no deep convection, the MOC strength is still over 50% of its maximum strength. The meridional heat transport is also slightly enhanced during periods of deep convection but maintains more than 50% of this maximum even when there is no convection. The system remains in the thermal mode even in the absence of deep convection because the warm boundary current continues to lose heat, both directly to the atmosphere and through eddy fluxes into the interior of the basin. The Ekman transport at the latitude of the sill will result in a northward heat transport of
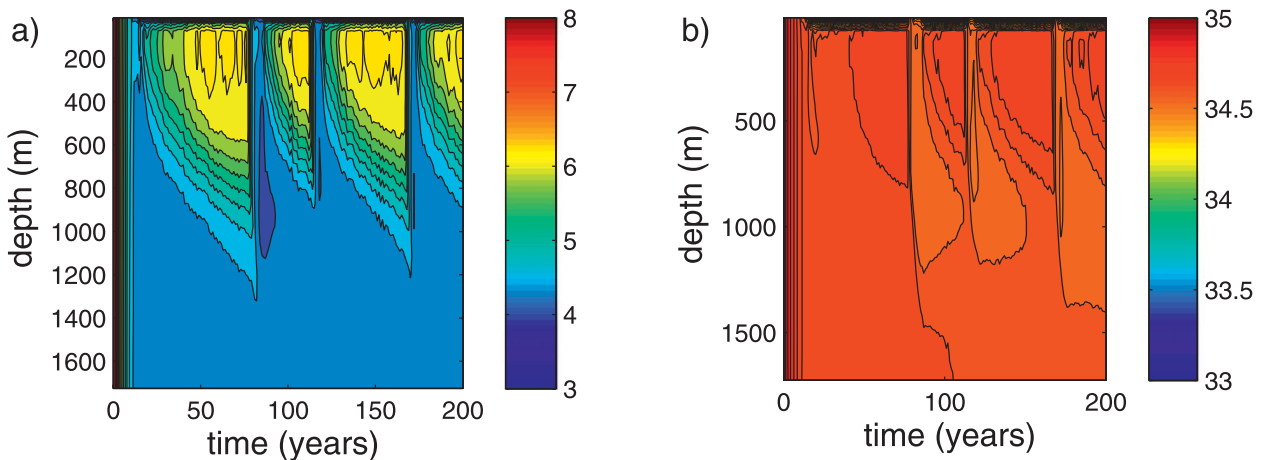

FIG. 9. Time–depth plot of the (a) temperature and (b) salinity averaged over the central 200 km of the basin interior for precipitation $E = -6 \times 10^{-8}$ m s^{-1} with $\mu/\epsilon = 0.44$ (run 12).
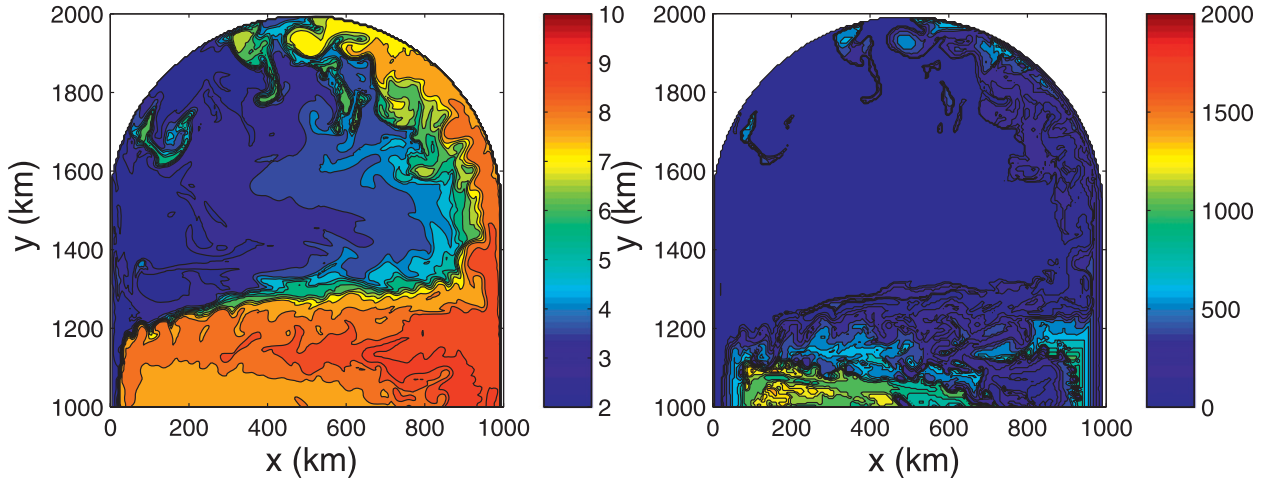
FIG. 10. Snapshot of (left) sea surface temperature and (right) mixed layer depth (defined as density anomaly 0.02 kg m^{-3} relative to the surface) for run 12.

approximately 6×10^{12} W, or about 10% of the total meridional heat transport in the model, so it is concluded that this is dominated by the geostrophic boundary current and not the northward flow in the Ekman layer.

The relative changes in deep convection, heat transport, and the meridional overturning circulation are shown as a function of precipitation in Fig. 12 for all of the model calculations in Table 1. Those calculations that result in a shutdown of deep convection have been run out to at least 50-yr integration time to make sure that no deep convection develops. The precipitation level is normalized by the theoretical prediction of the magnitude required to shut down deep convection E_c, as defined from the theory where $\Delta S = 0.5 \Delta T$. The diagnosed quantity plotted in each figure is normalized by its value in the absence of precipitation. The area of deep convection actually increases with increasing precipitation up until the critical level is reached, at which point deep convection is rapidly shut down (Fig. 12a). With increasing precipitation, the density anomaly of the convective waters decreases, and so the baroclinic transport of the boundary current also decreases. This makes the boundary current more stable, so fewer eddies are shed into the interior. It is these eddies that are responsible for restratification, so the weaker the eddy flux the larger the area that is open to deep convection. Just before shutdown, the area of deep convection is 50%–100% larger than it is in the absence of precipitation.

The ocean circulation remains in a thermally direct mode represented by the northward flow of warm water, sinking at high latitudes, and southward flow of cold water, even after deep convection has ceased. The strength of the meridional overturning circulation decreases slowly with increasing precipitation for values less than E_c. There is a sharp drop once deep convection ceases and

then a continued weaker decrease for values of $E > E_c$. The sense of the meridional overturning circulation remains the same even when the precipitation is double the value required to shut down deep convection.

The meridional heat flux shows even weaker dependence on the value of precipitation. The heat flux remains at 40%–80% of its value without precipitation even at the strongest values of freshwater forcing. This suggests that the atmosphere will be even less sensitive to the shutdown of deep convection than might be implied by the decrease in the meridional overturning strength. This weaker sensitivity is because most of the meridional heat transport at high latitudes is carried by the horizontal gyre, not the overturning gyre (Fanning and Weaver 1997; Pickart and Spall 2007).

The meridional density flux across the sill is shown in Fig. 12d. For low values of precipitation, the density flux is essentially the same as the heat flux. However, as precipitation increases the density flux rapidly decreases with nearly linear dependence on E/E_c. The sign of the net density flux across the sill changes from light water going into the marginal sea and denser water coming out
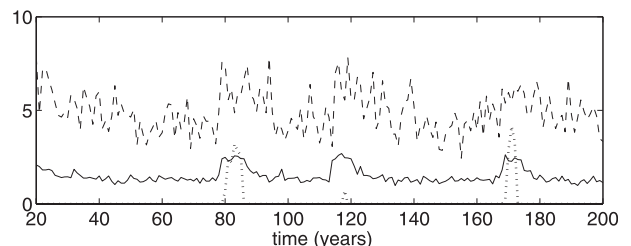

FIG. 11. Time series of the meridional overturning strength [Sv (1 Sv $\equiv 10^6$ m^3 s^{-1}); solid]; meridional heat transport (10^{13} W; dashed); and area of convection exceeding 1000-m depth (10^{11} m^2; dotted) for run 12.
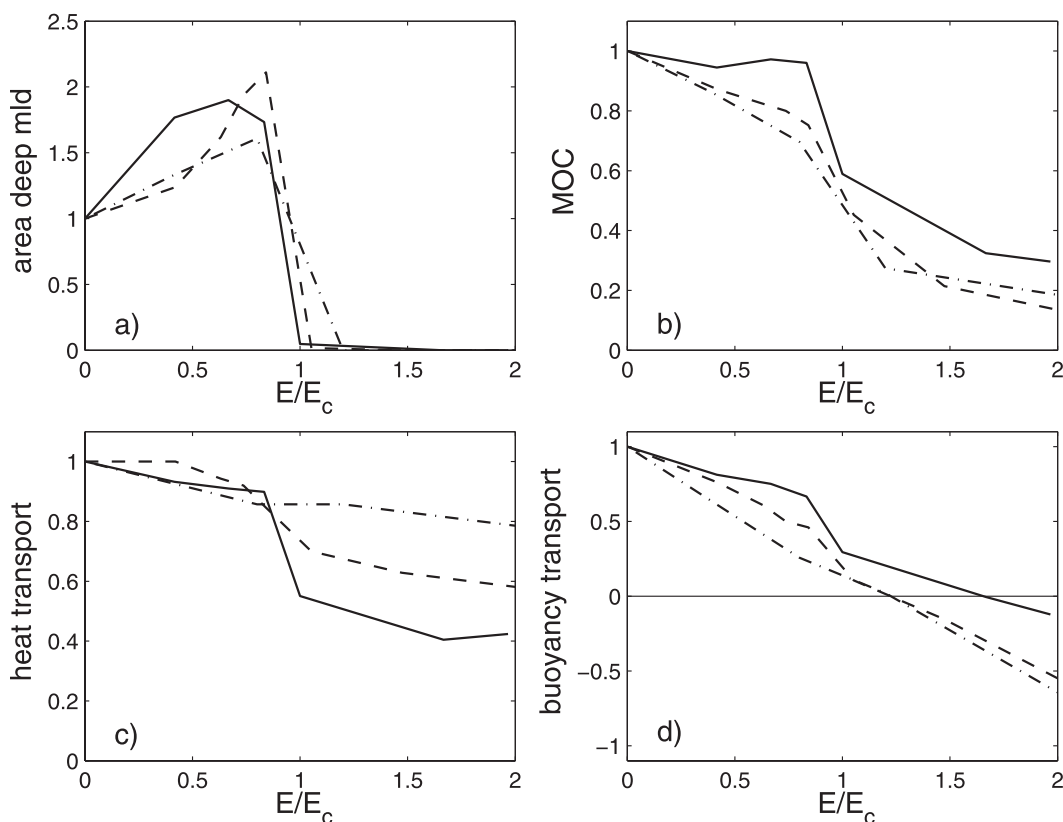
FIG. 12. Quantities as a function of precipitation (scaled by E_c, the theoretical magnitude required to shut down deep convection): (a) area of deep mixed layer depth (greater than 1000 m); (b) MOC; (c) meridional heat transport across the sill; and (d) meridional buoyancy transport across the sill. In each case, the ordinate is scaled by its value for no precipitation. Solid line is $\mu/\epsilon = 0.44$; dashed line is $\mu/\epsilon = 0.057$; and dashed–dotted line is $\mu/\epsilon = 0.022$.

(positive) to dense water going in and light water coming out (negative) for values of precipitation somewhat greater than E_c. The heat flux remains northward even as the outflowing water is lighter than the inflowing water.

The ocean state with no deep convection is not the same as Stommel's haline mode. In the haline mode both boxes are of uniform water properties, while for the no-convection state the marginal sea interior is strongly stratified with cold freshwater on top and warm, salty water below. The sense of the density exchange between the interior and the boundary current is different for the deep layer (eddies transport light water into the interior) than it is for the surface layer (eddies transport dense water into the interior). For very strong precipitation, the surface density exchange overwhelms the deep density exchange and the boundary current gets lighter within the basin.

5. Summary

The influences of precipitation on water mass transformation and deep convection in marginal seas are

studied using an analytic model and an idealized eddy-resolving ocean model. Two nondimensional numbers are identified that represent the relative influences of surface cooling, precipitation, and eddy fluxes on the state of the ocean. Two stable regimes are predicted. The thermal mode, analogous to the current circulation in the North Atlantic, has deep convection in the marginal sea, downwelling, and northward heat transport carried in a cyclonic boundary current. The second regime is a haline mode in which deep convection is not supported in the marginal sea and the circulation is in the opposite sense, anticyclonic around the marginal sea with a core of fresh and cold water in the interior. The analytic equations are the same as derived for the classic two-box models of the thermohaline circulation, although heat and freshwater transport in the present model are carried by eddy fluxes instead of the mean flow. The properties of the thermal mode predicted by the theory (temperature and salinity of the convective water and strength of the meridional overturning circulation) compare well with a series of eddy-resolving numerical model calculations in which various model

parameters are varied. The level of precipitation required to shut down deep convection is also well predicted by the theory, including its dependence on such parameters as the sill depth and the temperature of the water south of the sill.

For values of precipitation that exceed the critical value required to maintain deep convection, the numerical model remains in a thermally direct circulation (northward heat transport and downwelling at high latitudes). The baroclinic shear in the boundary current remains cyclonic in this regime because the light (fresh and cold) water in the basin interior remains trapped near the surface. The subsurface water is more dense than the water to the south of the sill, supporting northward flow of warm water along the eastern boundary and a northward heat transport. It is possible that reverse circulations characteristic of the haline mode could be supported by the numerical model, although none were found here. It was found that the heat transport is less sensitive to excessive precipitation than is the meridional overturning circulation. This is because the heat transport at high latitudes is carried primarily by the horizontal circulation in the cyclonic boundary current, not the overturning circulation (Fanning and Weaver 1997; Pickart and Spall 2007). The finding that the area of deep convection is maximum for precipitation just below the critical level further indicates that the extent of deep convection is not a good indicator of the state of the meridional overturning circulation or its proximity to thermohaline collapse. A decrease in the temperature of waters supplied to the marginal sea from the south actually makes it more likely that convection will cease, not less likely as might be assumed because the inflowing water is more dense. This is because it is the density contrast between the boundary current and the interior that drives the lateral eddy fluxes and supplies the salty water to the regions of deep convection.

APPENDIX

Numerical Model Configuration

The numerical model used in this study is the MIT General Circulation Model (Marshall et al. 1997), which solves the hydrostatic primitive equations on a uniform Cartesian, staggered C grid with level vertical coordinates.

The model domain is 2000 km in meridional extent and 1000 km in zonal extent and has topography along the perimeter that slopes linearly from 50 m down to the bottom depth of 2000 m with a horizontal scale that varies from 140 km over most of the basin to 20 km along the northern boundary. There is also a sill, whose depth will be varied, located at 1200-km latitude. The Coriolis parameter varies linearly with latitude as $f = f_0 + \beta y$, where $f_0 = 1.2 \times 10^{-4} \text{ s}^{-1}$ and $\beta = 2 \times 10^{-11} \text{ m}^{-1} \text{ s}^{-1}$. The horizontal resolution is 5 km and there are 30 levels in the vertical, varying from 25 m near the surface to 200 m near the bottom.

The model is forced with a zonal wind stress as

$$\tau(x, y) = \tau_0 \cos(\pi y / L_y). \tag{A1}$$

All calculations are forced with a wind stress of maximum strength $\tau_0 = 0.15 \text{ N m}^{-2}$, which gives a maximum Ekman upwelling velocity of approximately 15 cm day^{-1}, close to the climatological mean in the interior of the Nordic Seas and in the eastern North Atlantic south of the sill (Furevik and Nilsen 2005). Spall (2011) found that the basic characteristics of the water mass transformation in the marginal sea were not sensitive to the presence of wind forcing, so the wind strength has not been varied here.

The surface heat flux in the model $Q*$ is calculated by restoring the upper-level temperature T toward a prescribed atmospheric temperature T_A as $Q* = (T - T_A)\Gamma$. The salinity of the upper model level everywhere north of the sill is changed by an amount equivalent to a freshwater flux of E. Because there is no actual flux of freshwater into the model ocean through the sea surface, this boundary conditions is referred to as a virtual salt flux.

The temperature in the southernmost 200 km is also restored toward a profile with uniform vertical stratification of $N^2 = (g/\rho_0)\partial\rho/\partial z = 2 \times 10^{-6} \text{ s}^{-2}$ and an upper-level temperature of 10°C with a time scale of 20 days (south of the bold dashed line in Fig. 3). Salinity is restored toward a uniform value of 35 within this region. This gives a first baroclinic deformation radius, based on the full ocean depth, of $L_d = NH/f_0 = 20$ km. This restoring is intended to represent the thermodynamic processes that maintain the stratification at low latitudes and assumes that whatever energy required to do so is available.

The model incorporates second-order vertical viscosity and diffusivity with coefficients of $10^{-5} \text{ m}^2 \text{ s}^{-1}$. The vertical diffusion is increased to 1000 m^2 s^{-1} for statically unstable conditions in order to represent vertical convection. Horizontal viscosity is parameterized as a second-order operator with the coefficient A_h determined by a Smagorinsky closure as $A_h = (\nu_s/\pi)^2\Delta^2[(u_x - v_y)^2 + (u_y + v_x)^2]^{1/2}$, where $\nu_s = 2.5$ is a nondimensional coefficient, Δ is the grid spacing, and u and v are the

horizontal velocities (subscripts indicate partial differentiation). Temperature and salinity are advected with a third-order direct space–time flux limiting scheme (MITgcm tracer advection option 33; http://mitgcm.org). There is no explicit horizontal diffusion of temperature or salinity. Density is linearly related to temperature and salinity as $\rho = \rho_0 + \alpha_S S - \alpha_T T$, where $\alpha_T = 0.2$ kg m^{-3} °C^{-1} is the thermal expansion coefficient and $\alpha_S = 0.8$ kg m^{-3} is the haline expansion coefficient.

REFERENCES

Broeker, W. S., D. M. Peteet, and D. Rind, 1985: Does the ocean-atmosphere system have more than one stable mode of operation? *Nature,* **315,** 21–26.

Bryan, F. O., 1986: High latitude salinity effects and inter-hemispheric thermohaline circulations. *Nature,* **323,** 301–304.

Cenedese, C., 2012: Downwelling in basins subject to buoyancy loss. *J. Phys. Oceanogr.,* in press.

Dee, D. P., and Coauthors, 2011: The ERA-Interim reanalysis: Configuration and performance of the data assimilation system. *Quart. J. Roy. Meteor. Soc.,* **137,** 553–597.

Fanning, A. F., and A. J. Weaver, 1997: A horizontal resolution and parameter sensitivity study of heat transport in an idealized coupled climate model. *J. Mar. Res.,* **10,** 2469–2478.

Furevik, T., and J. E. O. Nilsen, 2005: Large-scale atmospheric circulation variability and its impacts on the Nordic Seas ocean climate—A review. *The Nordic Seas: An Integrated Perspective, Geophys. Monogr.,* Vol. 158, Amer. Geophys. Union, 366 pp.

Haney, R. L., 1971: Surface thermal boundary condition for ocean circulation models. *J. Phys. Oceanogr.,* **1,** 241–248.

Huang, R. X., J. R. Luyten, and H. L. Stommel, 1992: Multiple equilibrium states in combined thermal and saline circulation. *J. Phys. Oceanogr.,* **22,** 231–246.

Iovino, D., F. Straneo, and M. A. Spall, 2008: On the effect of a sill on dense water formation in a marginal sea. *J. Mar. Res.,* **66,** 325–345.

Isachsen, P. E., 2011: Baroclinic instability and eddy tracer transport across sloping bottom topography: How well does a modified Eady model do in primitive equation simulations? *Ocean Modell.,* **39,** 183–199.

Kuhlbrodt, T., S. Titz, U. Feudel, and S. Rahmstorf, 2001: A simple model of seasonal open ocean convection. Part II: Labrador Sea stability and stochastic forcing. *Ocean Dyn.,* **52,** 36–49.

Lilly, J. M., and P. B. Rhines, 2002: Coherent eddies in the Labrador Sea observed from a mooring. *J. Phys. Oceanogr.,* **32,** 585–598.

Manabe, S., and R. Stouffer, 1995: Simulation of abrupt climate change induced by freshwater input to the North Atlantic Ocean. *Nature,* **378,** 165–167.

Marotzke, J., 2000: Abrupt climate change and thermohaline circulation: Mechanisms and predictability. *Proc. Natl. Acad. Sci. USA,* **97,** 1347–1350.

Marshall, J., and F. Schott, 1999: Open-ocean convection: Observations, theory, and models. *Rev. Geophys.,* **37,** 1–64.

——, C. Hill, L. Perelman, and A. Adcroft, 1997: Hydrostatic, quasi-hydrostatic, and non-hydrostatic ocean modeling. *J. Geophys. Res.,* **102,** 5733–5752.

Nilsson, J., and G. Walin, 2001: Freshwater forcing as a booster of thermohaline circulation. *Tellus,* **53A,** 629–641.

Orvik, K. A., and P. Niiler, 2002: Major pathways of Atlantic Water in the northern North Atlantic and Nordic Seas toward Arctic. *Geophys. Res. Lett.,* **29,** 1896, doi:10.1029/2002GL015002.

Pickart, R. S., and M. A. Spall, 2007: Impact of Labrador Sea convection on the North Atlantic meridional overturning circulation. *J. Phys. Oceanogr.,* **37,** 2207–2227.

Poulain, P.-M., A. Warn-Varnas, and P. P. Niiler, 1996: Near surface circulation of the Nordic Seas as measured by Lagrangian drifters. *J. Geophys. Res.,* **101,** 18 237–18 258.

Prater, M. D., 2002: Eddies in the Labrador Sea as observed by profiling RAFOS floats and remote sensing. *J. Phys. Oceanogr.,* **32,** 411–427.

Rahmstorf, S., 1995: Bifurcations of the Atlantic thermohaline circulation in response to changes in the hydrological cycle. *Nature,* **378,** 145–149.

——, 2001: A simple model of open ocean convection. *Ocean Dynamics,* **52,** 26–35.

——, and Coauthors, 2005: Thermohaline circulation hysteresis: A model intercomparison. *Geophys. Res. Lett.,* **32,** L23605, doi:10.1029/2005GL023655.

Rooth, C., 1982: Hydrology and ocean circulation. *Prog. Oceanogr.,* **11,** 131–149.

Schanze, J. J., R. W. Schmitt, and L. L. Yu, 2010: The global oceanic freshwater cycle: A state-of-the-art quantification. *J. Mar. Res.,* **68,** 569–595.

Seager, R., Y. Kushnir, and M. A. Cane, 1995: On heat flux boundary conditions for ocean models. *J. Phys. Oceanogr.,* **25,** 3219–3230.

Spall, M. A., 2004: Boundary currents and water mass transformation in marginal seas. *J. Phys. Oceanogr.,* **34,** 1197–1213.

——, 2010: Dynamics of downwelling in an eddy-resolving convective basin. *J. Phys. Oceanogr.,* **40,** 2341–2347.

——, 2011: On the role of eddies and surface forcing in the heat transport and overturning circulation in marginal sea. *J. Mar. Res.,* **24,** 4844–4858.

Stigebrandt, A., 1985: On the hydrographic and ice conditions in the northern North Atlantic during different phases of a glaciation cycle. *Palaeogeogr. Palaeoclimatol. Palaeoecol.,* **50,** 303–321.

Stommel, H., 1961: Thermohaline convection with two stable regimes of flow. *Tellus,* **13,** 224–230.

Straneo, F., 2006: Heat and freshwater transport through the central Labrador Sea. *J. Phys. Oceanogr.,* **36,** 606–628.

Visbeck, M., J. Marshall, and H. Jones, 1996: Dynamics of isolated convective regions in the ocean. *J. Phys. Oceanogr.,* **26,** 1721–1734.

Welander, P., 1982: A simple heat-salt oscillator. *Dyn. Atmos. Oceans,* **6,** 233–242.

Wentz, F. J., L. Ricciardulli, K. Hilburn, and C. Mears, 2007: How much more rain will global warming bring? *Science,* **317,** 233–235.

Whitehead, J. A., 1995: Thermohaline ocean processes and models. *Annu. Rev. Fluid Mech.,* **27,** 89–113.